Journal of Intelligent & Robotic Systems (2022) 104: 66
https://doi.org/10.1007/s10846-022-01588-2

REGULAR PAPER

Estimating Evapotranspiration of Pomegranate Trees Using Stochastic Configuration Networks (SCN) and UAV Multispectral Imagery

Haoyu Niu[1] · Tiebiao Zhao[1] · Dong Wang[2] · YangQuan Chen[1]

Received: 22 September 2020 / Accepted: 31 January 2022 / Published online: 30 March 2022
© The Author(s) 2022

Abstract

Evapotranspiration (ET) estimation is important in precision agriculture water management, such as evaluating soil moisture, drought monitoring, and assessing crop water stress. As a traditional method, evapotranspiration estimation using crop coefficient (K_c) has been commonly used. Since there are strong similarities between the K_c curve and the vegetation index curve, the crop coefficient K_c is usually estimated as a function of the vegetation index. Researchers have developed linear regression models for the K_c and the normalized difference vegetation index (NDVI), usually derived from satellite imagery. However, the spatial resolution of the satellite image is often insufficient for crops with clumped canopy structures, such as vines and trees. Therefore, in this article, the authors used Unmanned Aerial Vehicles (UAVs) to collect high-resolution multispectral imagery in a pomegranate orchard located at the USDA-ARS, San Joaquin Valley Agricultural Sciences Center, Parlier, CA. The K_c values were measured from a weighing lysimeter and the NDVI values were derived from UAV imagery. Then, the authors established a relationship between the NDVI and K_c by using a linear regression model and a stochastic configuration networks (SCN) model, respectively. Based on the research results, the linear regression model has an R^2 of 0.975 and RMSE of 0.05. The SCN regression model has an R^2 and RMSE value of 0.995 and 0.046, respectively. Compared with the linear regression model, the SCN model improved performance in predicting K_c from NDVI. Then, actual evapotranspiration was estimated and compared with lysimeter data in an experimental pomegranate orchard. The UAV imagery provided a spatial and tree-by-tree view of ET distribution.

Keywords Evapotranspiration · Unmanned aerial vehicles · NDVI · SCNs

A conference version of the submitted paper appeared in the Proceedings of the 2020 International Conference on Unmanned Aircraft Systems (ICUAS'20), Athens, Greece. All the research results are reproducible and the dataset is available upon request.

✉ Haoyu Niu
hniu2@ucmerced.edu

Tiebiao Zhao
tzhao3@ucmerced.edu

Dong Wang
dong.wang@usda.gov

YangQuan Chen
ychen53@ucmerced.edu

1 University of California, Merced, 5200 Lake Rd, Merced, CA 95340, USA

2 USDA-ARS Water Management Research Unit, San Joaquin Valley Agricultural Sciences Center, Parlier, CA 93648, USA

1 Introduction

Evapotranspiration (ET) estimation is important in precision agriculture water management [1, 2]. ET is known as the main outgoing water flux from the surface on the earth [3]. ET is a combination of two separate processes, evaporation and transpiration. Evaporation is the process whereby liquid water is converted to water vapor [4]. Then, the water vapor removes from the evaporating surface. Transpiration is the process of the vaporization of liquid water contained in plant tissues and the vapor removal to the atmosphere [4]. The following three steps constitute the current theory for transpiration. First, the conversion of liquid-phase water to vapor water causes canopy cooling from latent heat exchange. Thus, canopy temperature can be used as an indicator of ET. Second, diffusion of water vapor from inside plant stomata on the leaves to the surrounding atmosphere. Third, atmospheric air mixing by convection or diffusion transports vapor near the plant surfaces to the upper atmosphere or off-site away from the plant canopy. Usually, evaporation and transpiration occur simultaneously. There are direct and indirect methods for ET estimation. For direct methods, there are lysimeters [5] and water balance methods [6]. For indirect methods, there are energy balance methods [3], Pan evaporation methods [6, 7], and remote sensing methods [8]. For energy balance methods, Bowen ratio [9, 10] and eddy covariance [11] have been widely used for ET estimation.

Using crop coefficient (K_c) for ET estimation is a commonly used method for water irrigation management. The crop evapotranspiration (ET_c) is calculated by the K_c approach whereby the effect of the various weather conditions are incorporated into reference ET (ET_o) and the crop characteristics into the K_c [4]:

$$ET_c = K_c \times ET_o. \tag{1}$$

The curve of K_c is the crop coefficient distribution during a whole growing season. At the beginning of the growing season, K_c starts increasing from a small value. When the canopy cover is full, the K_c reaches a maximum around the mid-season. Then, the K_c starts decreasing before the end of the growing season.

The normalized difference vegetation index (NDVI) has been widely used for vegetation monitoring, such as water stress detection [12, 13], crop yield assessment [14], and ET estimation [15, 16]. The NDVI is calculated by

$$NDVI = \frac{\rho_{NIR} - \rho_R}{\rho_{NIR} + \rho_R}, \tag{2}$$

where ρ_{NIR} is the reflectance of the near-infrared band. The parameter ρ_R is the reflectance for the red waveband. NDVI is a standardized method to measure healthy vegetation. When the NDVI has a higher value, it means the vegetation has a high level of photosynthesis.

Estimating crop coefficient values using satellite-derived NDVI has been commonly used in many studies. [17–19]. For instance, Trout et al. [20] and Zhang et al. [21] used NDVI to estimate canopy ground cover for generating K_c. Kamble et al. [17] established a relationship between NDVI and K_c by linear regression model. Although satellite images can provide spatially distributed measurements, they cannot acquire useful spatio-temporal resolution imagery for precision agriculture applications [22]. The satellite overpass time is not always consistent with research requirements. For example, the Landsat 8 visible and near-infrared image resolution is at the 30-meter level, with a 16-day revisit time. The thermal band resolution for the Landsat is at a 100-meter level. Some other satellites, such as GOES and MODIS, also have thermal sensors. The thermal imagery provided by MODIS is 500 m per pixel. The GOES has a thermal resolution of 5 km per pixel. For many agricultural applications, the revisit time and resolution are unacceptable when considering the weather conditions, such as cloud cover. The spatial resolution may also not be available for detecting the field variability [23] and is only useful for large scale studies. Although there are new satellite platforms, such as Sentinel-2, which provide a significant improvement in revisit time and multispectral capability, the timing of satellite overpass is not always synchronous with research requirements [24].

As a new remote sensing platform, researchers are more and more interested in the potential of small UAVs in precision agriculture [25–28], especially on heterogeneous crops, such as vineyard and orchards [29, 30]. Compared with the satellite, UAVs can be operated at any time if the weather is within operating limitations. The satellite has a fixed flight path, UAVs are more mobile and adaptive for site selection. Mounted on the UAVs, lightweight sensors, such as RGB cameras, multispectral cameras, and thermal infrared cameras, can be used to collect high-resolution images. The higher temporal and spatial resolution images, relatively low operational costs, and nearly real-time image acquisition make the UAVs ideal for mapping and monitoring ET.

The contribution of this research was to investigate the methods for estimating K_c and ET using UAV-based NDVI for an experimental pomegranate orchard. The novelty is that a regression model was established between the NDVI and K_c by using the SCN algorithm, which was first proposed by the authors. The pomegranate has been widely planted in the world. The pomegranate also has drought resistance and high economic value. There is approximately 11,000 ha of pomegranate in the semi-arid and arid areas of California [21]. The spatial and temporal variability of K_c and NDVI were analyzed by using the SCN model, which made tree-by-tree ET estimation becomes possible. The performance of the proposed regression model was evaluated by the data collected by the UAVs.

The rest of the paper is organized as follows. Section 2 introduces MATERIAL AND METHODS for ET estimation, such as the pomegranate study site, the UAV platform and sensors being used, UAV image processing technology, and the SCNs. Results and discussions are presented in Section 3. A simple regression model and SCN model are used to demonstrate the ET estimation method. In Section 4, concluding remarks are presented.

Fig. 1 Pomegranate test site. This research was conducted in an experimental pomegranate orchard at the USDA-ARS, San Joaquin Valley Agricultural Sciences Center (36.594 °N, 119.512 °W), Parlier, California, 93648, USA. There were two weighing lysimeters [21], which are 2 m × 4 m by 3 m deep

2 Material and Methods

2.1 Pomegranate Study Site

This research was conducted in an experimental pomegranate orchard at the USDA-ARS, San Joaquin Valley Agricultural Sciences Center (36.594 °N, 119.512 °W), Parlier, California, 93648, USA (Fig. 1). There are two weighing lysimeters [21], which are 2 m × 4 m by 3 m deep. The lysimeters have a resolution of 0.1 mm of water loss, which is located in the center of the field, marked in red boxes in Fig. 1. The pomegranate was planted in 2010 with a 5 m spacing between rows and 2.75 m within-row tree spacing in a 1.3 ha field.

2.2 The UAV Platform and Multispectral Camera

In this research, the authors used a UAV platform, called "Hover" (Fig. 2). The "Hover" was equipped with a Pixhawk flight controller, GPS, telemetry antennas. It can fly over the field by waypoints mode (designed by using Mission Planner software). The lithium polymer battery has a capacity of 9500 mAh, which can support a 30-minute flight mission with cameras mounted on it. The "Hover"

Fig. 2 The "Hover". The "Hover" was equipped with a Pixhawk flight controller, GPS, telemetry antennas. It can fly over the field by waypoints mode (designed by using Mission Planner software). The lithium polymer battery has a capacity of 9500 mAh, which can support a 30-minute flight mission with cameras mounted on it

Table 1 The UAV flight schedule

Dates	Flight time	Flight height
May 8^{th}, 2019	12 - 1 pm	60 m,
Jun 5^{th}, 2019	12 - 1 pm	60 m,
Jul 25^{th}, 2019	12 - 1 pm	60 m,
Aug 7^{th}, 2019	12 - 1 pm	60 m,
Aug 29^{th}, 2019	12 - 1 pm	60 m,
Sep 19^{th}, 2019	12 - 1 pm	60 m,
Oct 3^{rd}, 2019	12 - 1 pm	60 m,
Oct 29^{th}, 2019	12 - 1 pm	60 m.

The flight height was set up as 60 m. The overlapping of UAV imagery was set up as 80%, so that the UAV imagery of the pomegranate can be stitched together during image processing. A bi-weekly UAV flight schedule is suggested to collect sufficient data

is equipped with high efficient power system, including T-Motor MN3508 KV380 motor, 1552 folding propeller and Foxtech Multi-Pal 40A OPTP ESC, to ensure long flight time.

The Rededge M camera (MicaSense, Seattle, WA, USA) was being used for collecting the multispectral imagery, which had five different bands. The five bands are Blue, Green, Red, Near-infrared, and Red edge. The Rededge M also has a spectral resolution of 1280 × 960 pixel, with a 46° field of view. With a Downwelling Light Sensor (DLS), which is a 5-band light sensor that connects to the camera, the Rededge M can measure the ambient light during a flight mission for the five bands. Then, the DLS can record the light information in the metadata of the images captured by the camera. After the image calibration, the information detected by the DLS can be used for correcting lighting changes during a flight, such as changes in cloud cover during a UAV flight.

2.3 UAV Image Collection and Processing

The authors used the Mission Planner to program all flight missions. The flight height was set up as 60 m. The overlapping of UAV imagery was set up as 80%, so that the UAV imagery of the pomegranate could be stitched together during image processing. A bi-weekly UAV flight schedule was suggested to collect sufficient data. If there is a UAV crash, unexpected weather conditions, hardware issues, or unknown reasons, data may not be collected successfully. If data is missed, people may have to wait for another year. Therefore, the authors flew the UAV bi-weekly over the pomegranate field at noon during the growing season in 2019 (Table 1).

To minimize the shading effect on the images, the UAVs are usually flying at noon with clear sky conditions. Because each pixel in a UAV image is a percentage of the reflected light, pixel values need to be calibrated by using a known reflectance value. Therefore, the image of a calibration board needs to be taken before and after the flight missions, servicing as the reflectance reference (Fig. 3). It is important to take pictures of the reference panel immediately before and after the flight missions because the solar angle and light intensity can change [12], which causes inaccurate experiment results. UAV images usually have higher radiometric homogeneity than aircraft or satellite images because of the lower flight altitude [31]. However, there are also special UAVs image quality problems. For

Fig. 3 The image of a calibration board needs to be taken before and after the flight missions, servicing as the reflectance reference. It is important to take pictures of the reference panel immediately before and after the flight missions because the solar angle and light intensity can change [12], which causes inaccurate experiment results. UAV images usually have higher radiometric homogeneity than aircraft or satellite images because of the lower flight altitude [31]

Table 2 Orthomosaic images generation workflow in Agisoft Metashape

Step 1 : Align Photos	Step 2 : Build Mesh	Step 3 : Build Orthomosaick
Accuracy: Medium	Surface type: Height field (2.5D)	Type: Planar
Generic preselection: Yes	Source data: Sparse cloud	Projection plane: TOP XY
Key point limit: 40,000	Face count: Medium (30,000)	Rotation angle: 0
Tie point limit: 4,000	Interpolation: Enabled (default)	Surface: Mesh
Adaptive camera model fitting: No	Point classes: All	Blending mode: Mosaic (default)
	Caculate vertex colors: Yes	Enable hole filling: Yes
		Enable back-face culling: No

example, the camera position on the UAVs might be different for each flight mission, which can cause different spatial resolution or different viewing angles [31]. The low flight height of UAVs can also result in geometric distortion [31, 32]. Besides, lower flight height results in greater numbers of UAV images to keep effective overlapping, which makes image processing more time-consuming.

After the flight missions, all of the aerial images were stitched together to generate the orthomosaick images (Table 2, and Fig. 4) in Metashape (Agisoft LLC, Russian). Preselection is recommended because it can speed up the processing of large datasets. Building the dense cloud can reconstruct a more accurate surface, which can improve the quality of the final orthomosaic. Higher quality usually can result in a more accurate surface, which means a greater number of points. However, higher quality is not recommended because of longer data processing time. Medium quality is sufficient for UAVs image processing, especially for low variations field. Building Digital Elevation Model (DEM) allows generating an accurate surface, which can be used as a source for the orthomosaic generation. This will shorten the data processing time compared with Build Mesh operation because Build Mesh is usually used for a more complex surface. he source data for building DEM is the dense cloud. For the interpolation method, **Extrapolated** option is selected because it can generate a surface without gaps being extrapolated to the bound box sides. The default option for **Interpolation** is **Enabled**, which is not recommended because it will leave the valid elevation values only for fields that are seen from at least one aligned camera.

2.4 Stochastic Configuration Networks (SCNs)

The stochastic configuration networks (SCNs) was proposed by Wang et al. in 2017 [33]. The SCNs has a powerful capability for regression and classification analysis. Traditionally, it is quite challenging to correctly determine an appropriate architecture for a neural network so that the trained model can achieve excellent performance for both learning and generalization. Compared with the known randomized learning algorithms for neural networks, the SCNs randomly assign the input weights and biases of the hidden nodes in the light of a supervisory mechanism. Randomness plays a significant role in both exploration and exploitation. A good neural networks architecture with randomly

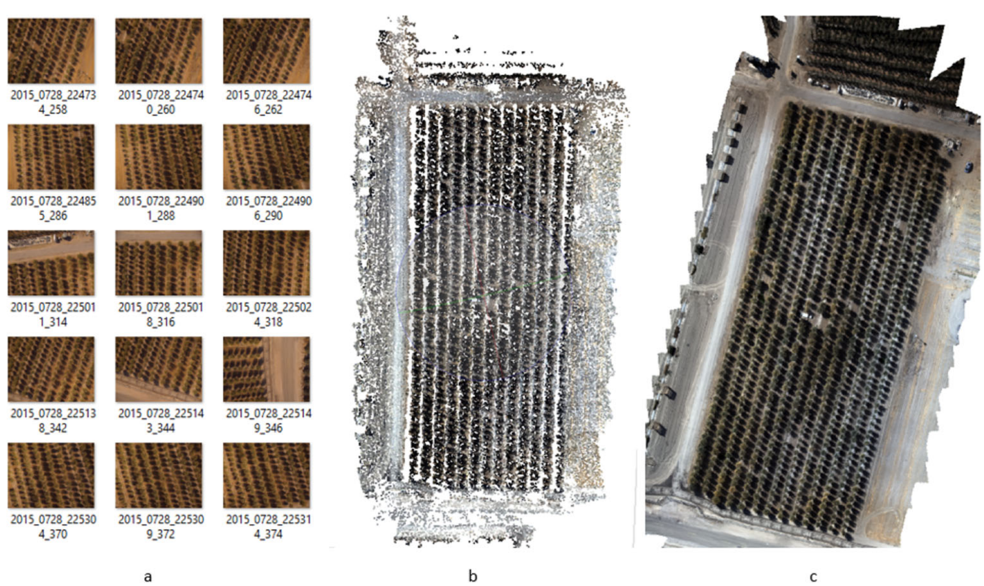

Fig. 4 Agisoft Metashape image processing workflow (**a**) Align Photos. **b** Build Mesh. **c** Generate orthomosaick

Table 3 The SCNs model with parameter

Properties	Values
Name:	'Stochastic Configuration Networks'
version:	'1.0 beta'
L:	4
W:	[0.4924 -0.4987 -4.3543 9.2007]
b:	[-0.4650 -0.4197 -4.7048 -9.2846]
Beta:	[4 x 1 double]
r:	[0.9000 0.9900 0.9990 0.9999 1.0000 1.0000]
tol:	1.0000e-03
Lambdas:	[0.5000 1 5 10 30 50 100 150 200 250]
L_{max}:	250
T_{max}:	100
nB:	1
verbose:	50
COST:	5.5250e-13

For example, the maximum times of random configuration T_{max} was set as 100. The scale factor Lambdas in the activation function, which directly determined the range for the random parameters, was examined by performing different settings (0.5 - 200). The tolerance was set as 0.001. For the other parameters in the SCNs model, please refer to [33]

assigned weights can easily outperform a poorer architecture with finely tuned weights [34, 35]. The output weights are analytically evaluated in a constructive or selective method. In contrast with the known randomized learning algorithms, such as the Randomized Radial Basis Function (RBF) Networks [36] and the Random Vector Functional-link (RVFL) [37], SCNs can provide good generalization performance at a faster speed. Concretely, there are three types of SCNs algorithms, which are SC-I, SC-II, and SC-III. SC-I algorithm uses a constructive scheme to evaluate the output weights only for the newly added hidden node [38]. All of the previously obtained output weights are kept the same. The SC-II algorithm recalculates part of the current output weights by analyzing a local least squares problem with user-defined shifting window size. The SC-III algorithm finds all the output weights together by solving a global least-squares problem. SCNs algorithms have been widely used in many areas such as image data analytics [16, 39], prediction of component concentrations in sodium aluminate liquor [40], and etc. [41, 42].

The linear regression can only plot the best fit line, but the data may have a non-linear pattern. Therefore, in this research, the SCNs is applied to derive better regression model than the linear regression model.

3 Results and Discussion

3.1 Seasonal K_c and *NDVI*

The values of K_c and NDVI were shown in Fig. 5. The values of K_c were derived using (1). The ET_c was recorded by the weighing lysimeter in the center of the pomegranate field. The ET_o was calculated by the California Irrigation Management Information System

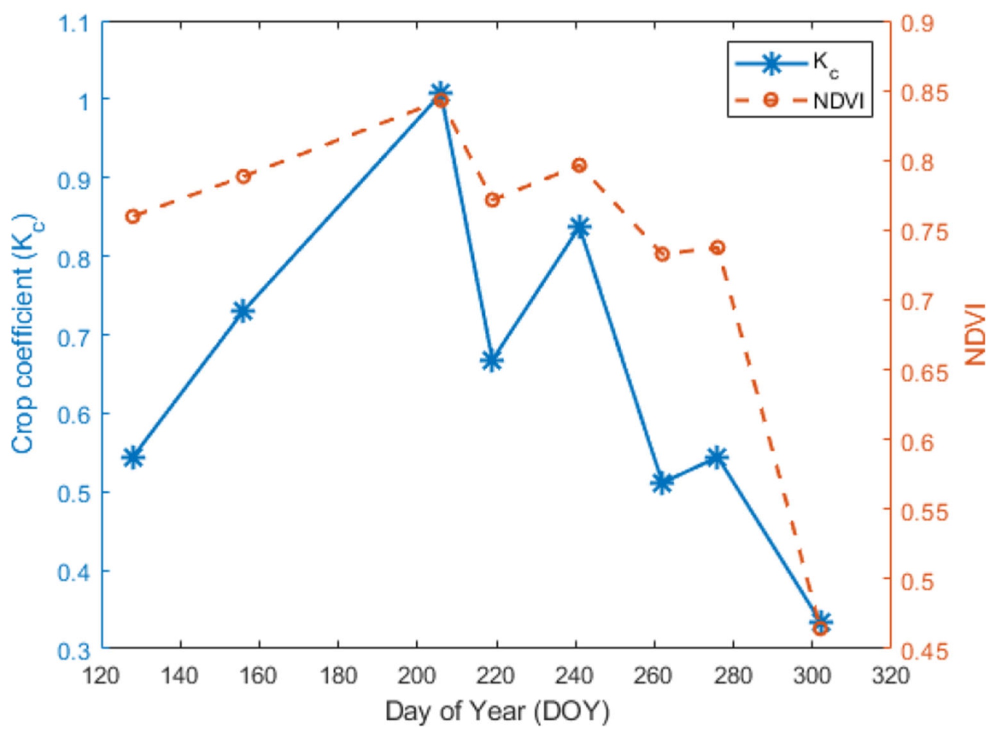

Fig. 5 Seasonal K_c and NDVI at the pomegranate field in 2019. The values of K_c were derived using equation (1). The ET_c was recorded by the weighing lysimeter in the center of the pomegranate field. The ET_o was calculated by the California Irrigation Management Information System (CIMIS) near the pomegranate field. The NDVI was derived by image processing tools in MATLAB 2020b

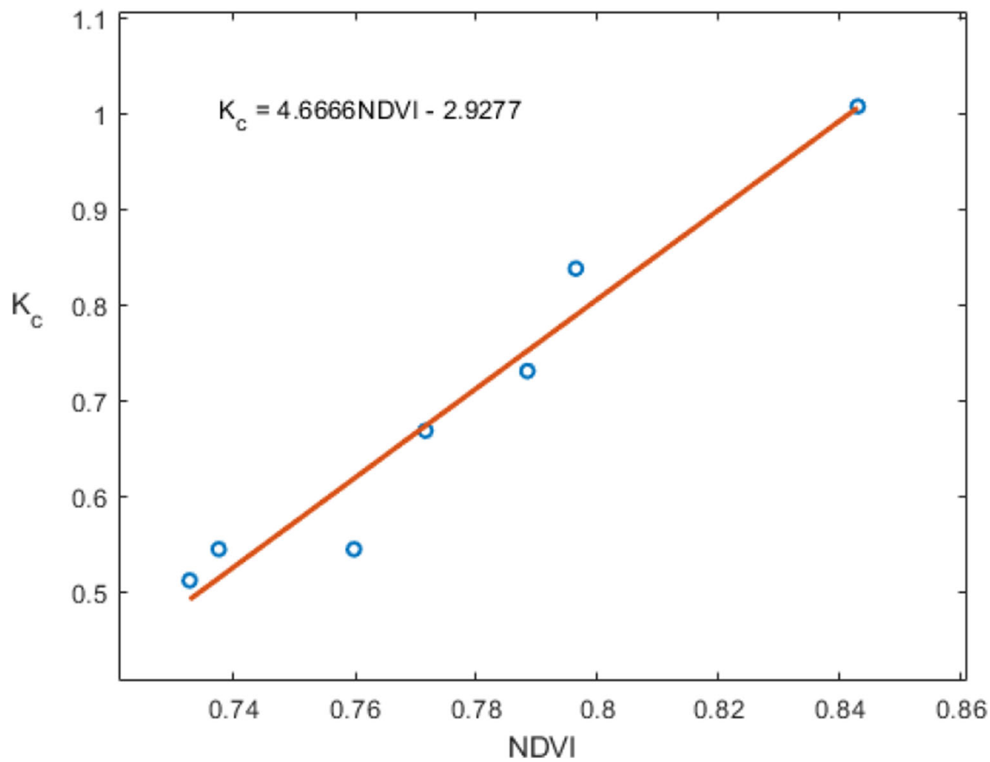

Fig. 6 Linear regression model for K_c and NDVI. There was a strong correlation between the K_c and NDVI. A simple linear regression model was built using the NDVI values derived from the UAV imagery and the K_c from field measurement

(CIMIS) near the pomegranate field. The NDVI was derived by image processing tools in MATLAB 2020b.

A strong correlation was shown between the K_c and NDVI during the growing season in 2019. The maximum values of K_c and NDVI were 1.0069 and 0.8429 on July 25^{th} (DOY 206), respectively. The high values of K_c and NDVI showed that the trees in the lysimeter were in a well-irrigated condition. The K_c increased fast at the beginning

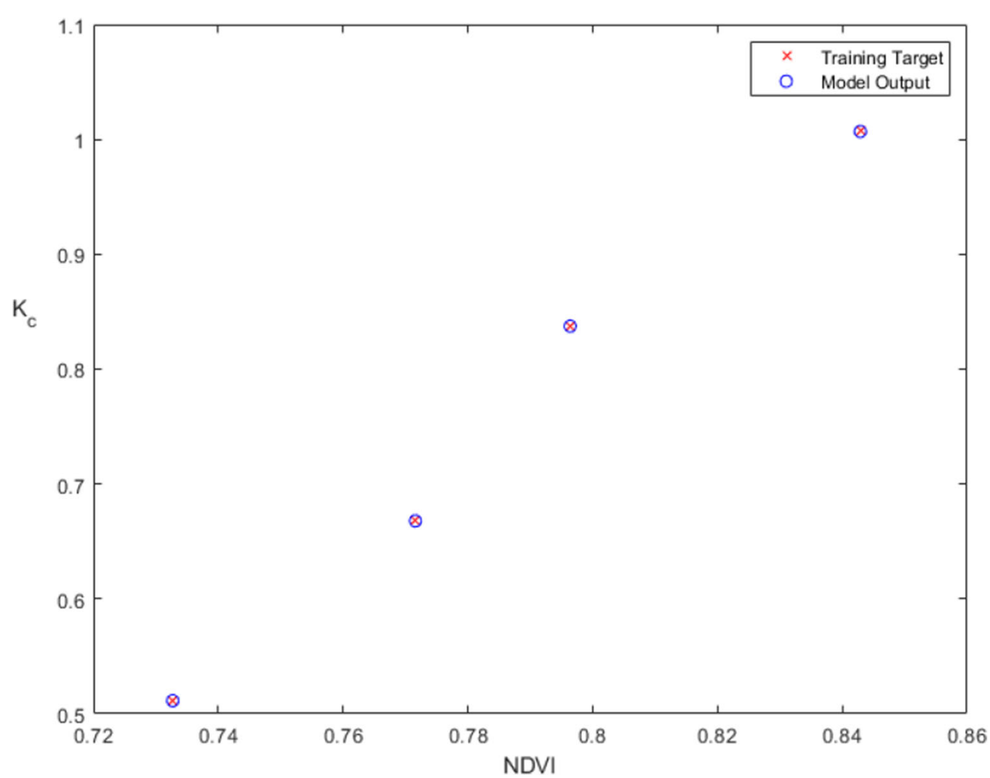

Fig. 7 The SCNs training model performance. Since the dataset of K_c and NDVI was not large, in this study, SCNs model was used for building the regression model between K_c and NDVI. Four out of seven days of data were used for training the SCNs regression model. All the data points were fitted very well in the trained model

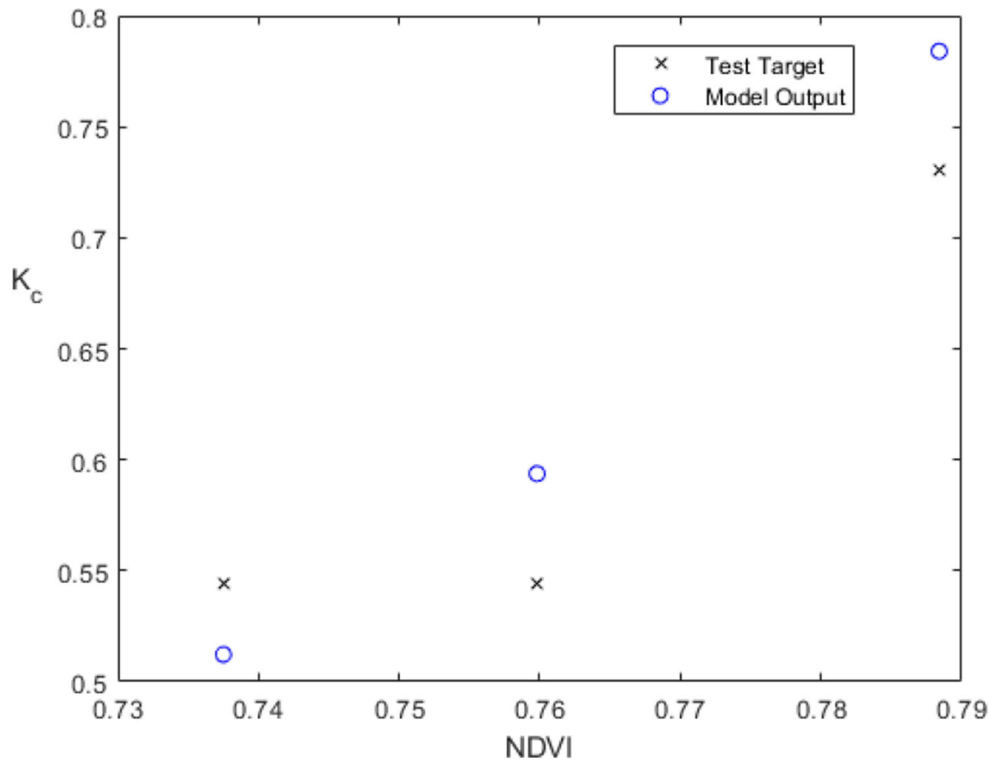

Fig. 8 The SCNs model evaluation performance. Three days of data were used to evaluate the trained model. The value of R^2 was 0.995. The value of RSME was 0.046. Both of them showed good performance for estimating K_c by using NDVI. The variations of K_c were well explained by using the NDVI from UAV images

of the growing season. After the peak of the mid-season, K_c started decreasing. Both K_c and NDVI had very low values on October 29^{th} (DOY 302). The reason was that most leaves fell off the pomegranate trees after the harvest. Therefore, the data of DOY 302 was not used for the data analysis.

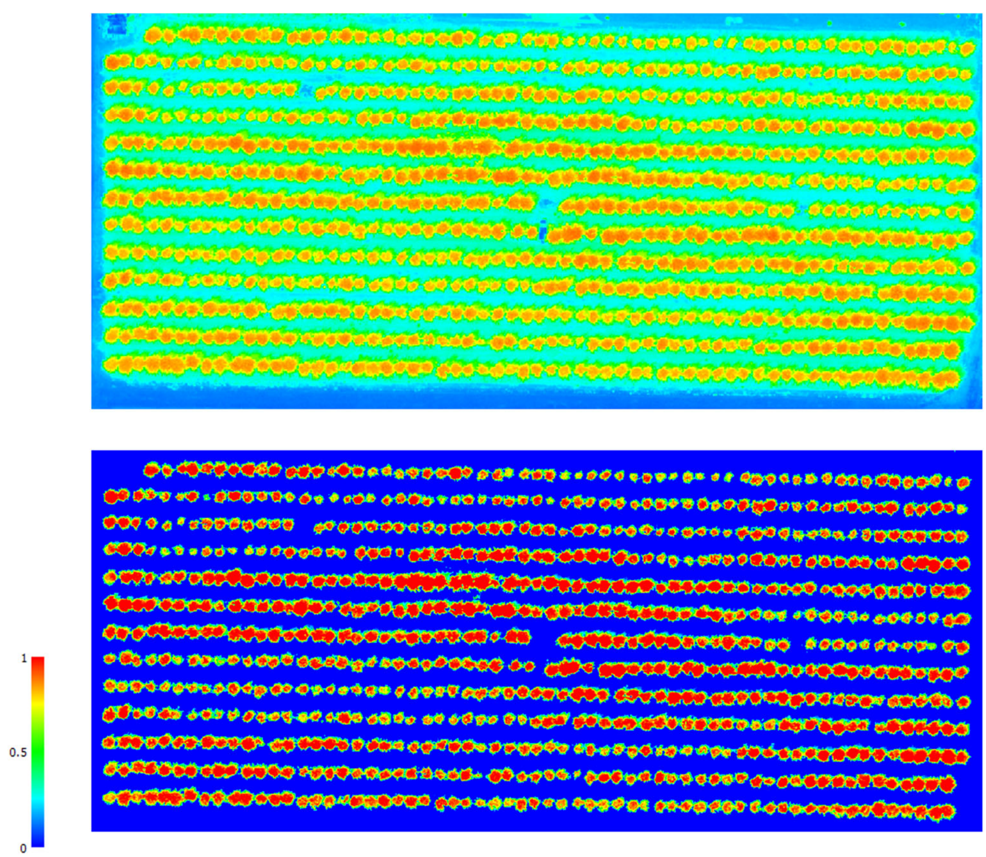

Fig. 9 NDVI (top) and K_c (bottom) maps of the pomegranate using UAVs. (Sept. 19^{th}, 2019)

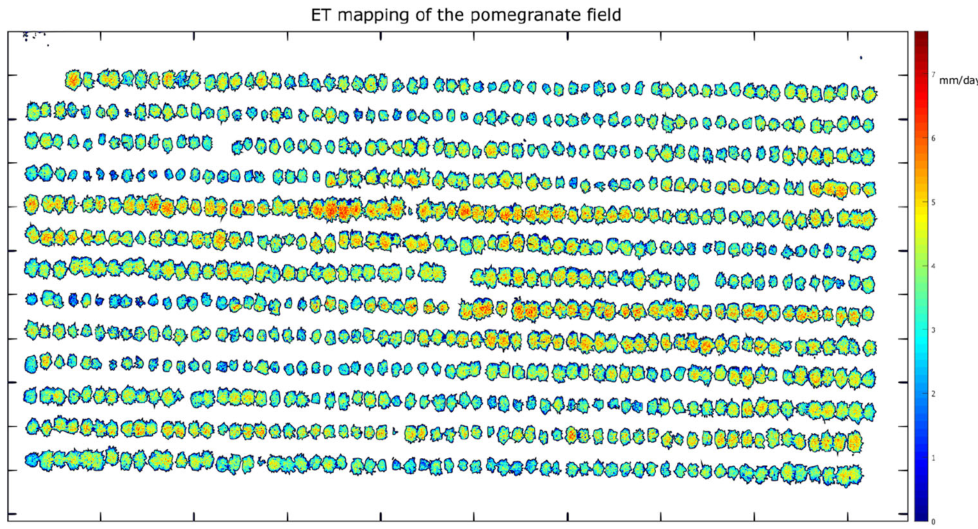

Fig. 10 ET mapping of the pomegranate. (Sept. 19^{th}, 2019)

3.2 Regression Models for K_c and NDVI

As shown in Fig. 6, there was a strong correlation between the K_c and NDVI. A simple linear regression model was built using the NDVI values derived from the UAV imagery and the K_c from field measurement,

$$K_c(NDVI) = 4.6666NDVI - 2.9277, \tag{3}$$

where 4.6666 and -2.9277 were the slope and intercept coefficients, respectively. The correlation coefficient (R^2) was 0.975. The root mean square error (RSME) was 0.05.

With the development of machine learning technology, many neural networks have been applied for agricultural applications [30, 43]. Since the dataset of K_c and NDVI was not large, in this study, SCNs was used for building the regression model between K_c and NDVI. Four out of seven days of data were used for training the SCNs regression model. All the data points were fitted very well in the trained model, as shown in Fig. 7. The weights and bias were shown in Table 3. The parameter L meant that there were four hidden nodes of the trained SCNs model. For the other parameters in the SCNs model, please refer to [33].

Three days of data were used to evaluate the trained model, as shown in Fig. 8. The value of R^2 was 0.995. The value of RSME was 0.046. Both of them showed good performance for estimating K_c by using NDVI. The variations of K_c were well explained by using the NDVI from UAV images. The trained model was used to generate the K_c. For example, the spatial mapping of NDVI and K_c on September 19^{th} were shown in Fig. 9. The spatial mapping of ET on September 19^{th} was shown in Fig. 10.

4 Conclusions

In this article, UAV flight missions were conducted to collect remote sensing multispectral images in a pomegranate orchard at USDA. Using the NDVI derived from the multispectral imagery, the authors could apply a SCNs for a regression model between NDVI and K_c. The parameters of the SCNs model was shown in Table 3. The K_c represented the actual growth conditions in the field. Therefore, K_c could be used for estimating the ET temporally and spatially in the pomegranate field.

The simple linear regression model was $K_c(NDVI) = 4.6666NDVI - 2.9277$. Compared with the simple linear regression model, the SCNs model could better fit the data points in the training dataset. The simple linear regression model had R^2 and RMSE of 0.975 and 0.05, respectively. The SCNs regression model had R^2 and RMSE of 0.995 and 0.046. The SCNs showed a better performance than the linear regression model.

Although only the data of 2019 was used for analysis, the study had provided evidence that variations of NDVI from UAV imagery could be used to explain the variations of K_c. In the future, the data of 2017 and 2018 will be added to train a more robust SCNs model.

Acknowledgements Thanks go to Stella Zambrzuski, Joshua Ahmed, and Christopher Currier for flying drones and collecting field measurements.

Open Access This article is licensed under a Creative Commons Attribution 4.0 International License, which permits use, sharing, adaptation, distribution and reproduction in any medium or format, as long as you give appropriate credit to the original author(s) and the source, provide a link to the Creative Commons licence, and indicate if changes were made. The images or other third party material in this article are included in the article's Creative Commons licence, unless indicated otherwise in a credit line to the material. If material is not included in the article's Creative Commons licence and your intended use is not permitted by statutory regulation or exceeds the permitted use, you will need to obtain permission directly from the copyright holder. To view a copy of this licence, visit http://creativecommons.org/licenses/by/4.0/.

References

1. Niu, H., Zhao, T., Wei, J., Wang, D., Chen, Y.: Reliable tree-level evapotranspiration estimation of pomegranate trees using lysimeter and UAV multispectral imagery, in 2021. In: IEEE Conference on Technologies for Sustainability (SusTech), pp. 1–6. IEEE (2021)
2. Niu, H., Hollenbeck, D., Zhao, T., Wang, D., Chen, Y.: Evapotranspiration estimation with small UAVs in precision agriculture. Sensors **20**(22), 6427 (2020)
3. Liou, Y.-A., Kar, S.: Evapotranspiration estimation with remote sensing and various surface energy balance algorithms—A review. Energies **7**, 5 (2014)
4. Allen, R.G., Pereira, L.S., Raes, D., Smith, M.: FAO irrigation and drainage paper No. 56, Rome: Food and Agriculture Organization of the United Nations **56**, 97 (1998)
5. Liu, C., Zhang, X., Zhang, Y.: Determination of daily evaporation and evapotranspiration of winter wheat and maize by large-scale weighing lysimeter and micro-lysimeter. Agr. Forest. Meteorol. **111**(2), 109–120 (2002)
6. Xu, C.-Y., Singh, V.: Evaluation of three complementary relationship evapotranspiration models by water balance approach to estimate actual regional evapotranspiration in different climatic regions. J. Hydrol. **308**(1-4), 105–121 (2005)
7. Grismer, M.E., Orang, M., Snyder, R., Matyac, R.: Pan evaporation to reference evapotranspiration conversion methods. J. Irrig. Drain. Eng. **128**(3), 180–184 (2002)
8. Allen, R., Irmak, A., Trezza, R., Hendrickx, J.M., Bastiaanssen, W., Kjaersgaard, J.: Satellite-based ET estimation in agriculture using SEBAL and METRIC. Hydrol. Process. **25**, 26 (2011)
9. Angus, D., Watts, P.: Evapotranspiration-How good is the Bowen ratio method? In: Developments in Agricultural and Managed Forest Ecology, vol. 13, pp. 133–150. Elsevier (1984)
10. Fritschen, L.J.: Accuracy of evapotranspiration determinations by the Bowen ratio method. Hydrol. Sci. J. **10**(2), 38–48 (1965)
11. Nagler, P.L., Scott, R.L., Westenburg, C., Cleverly, J.R., Glenn, E.P., Huete, A.R.: Evapotranspiration on western US rivers estimated using the enhanced vegetation index from MODIS and data from eddy covariance and Bowen ratio flux towers. Remote Sens. Environ. **97**(3), 337–351 (2005)
12. Zhao, T., Stark, B., Chen, Y., Ray, A.L., Doll, D.: A detailed field study of direct correlations between ground truth crop water stress and normalized difference vegetation index (NDVI) from small unmanned aerial system (sUAS). In: 2015 International Conference on Unmanned Aircraft Systems (ICUAS), pp. 520–525. IEEE (2015)
13. Zhao, T., Doll, D., Chen, Y.: Better almond water stress monitoring using fractional-order moments of non-normalized difference vegetation index. In: 2017 ASABE Annual International Meeting American Society of Agricultural and Biological Engineers (2017)
14. Zhao, T., Wang, Z., Yang, Q., Chen, Y.: Melon yield prediction using small unmanned aerial vehicles. In: Autonomous Air and Ground Sensing Systems for Agricultural Optimization and Phenotyping II International Society for Optics and Photonics (2017)
15. Niu, H., Zhao, T., Wang, D., Chen, Y.: Estimating evapotranspiration with UAVs in agriculture: A review. In: 2019 ASABE Annual International Meeting American Society of Agricultural and Biological Engineers (2019)
16. Niu, H., Wang, D., Chen, Y.: Estimating actual crop evapotranspiration using deep stochastic configuration networks model and UAV-based crop coefficients in a pomegranate orchard. In: Autonomous Air and Ground Sensing Systems for Agricultural Optimization and Phenotyping V International Society for Optics and Photonics (2020)
17. Kamble, B., Kilic, A., Hubbard, K.: Estimating crop coefficients using remote sensing-based vegetation index. Remote Sens. **5**(4), 1588–1602 (2013)
18. Reyes-Gonzalez, A., Hay, C., Kjaersgaard, J., Neale, C.: Use of remote sensing to generate crop coefficient and estimate actual crop evapotranspiration. In: 2015 ASABE Annual International Meeting American Society of Agricultural and Biological Engineers, p 1 (2015)
19. Hunsaker, D.J., Pinter, P.J., Barnes, E.M., Kimball, B.A.: Estimating cotton evapotranspiration crop coefficients with a multispectral vegetation index. Irrig. Sci. **22**(2), 95–104 (2003)
20. Trout, T.J., Johnson, L.F., Gartung, J.: Remote sensing of canopy cover in horticultural crops. HortSci. **43**(2), 333–337 (2008)
21. Zhang, H., Anderson, R.G., Wang, D.: Satellite-based crop coefficient and regional water use estimates for Hawaiian sugarcane. Field Crop Res **180**, 143–154 (2015)
22. Ershadi, A., McCabe, M.F., Evans, J.P., Walker, J.P.: Effects of spatial aggregation on the multi-scale estimation of evapotranspiration. Remote Sens. Environ. **131**, 51–62 (2013)
23. McCabe, M., Balick, L., Theiler, J., Gillespie, A., Mushkin, A.: Linear mixing in thermal infrared temperature retrieval. Int. J. Remote Sens. **29**(17-18), 5047–5061 (2008)
24. Cammalleri, C., Anderson, M., Gao, F., Hain, C., Kustas, W.: A data fusion approach for mapping daily evapotranspiration at field scale. Water Resour. Res. **49**(8), 4672–4686 (2013)
25. Díaz-Varela, R., de la Rosa, R., León, L., Zarco-Tejada, P.: High-resolution airborne UAV imagery to assess olive tree crown parameters using 3D photo reconstruction: Application in breeding trials. Remote Sensing **7**, 4 (2015)
26. Gonzalez-Dugo, V., Goldhamer, D., Zarco-Tejada, P.J., Fereres, E.: Improving the precision of irrigation in a pistachio farm using an unmanned airborne thermal system. Irrig. Sci. **33**(1), 43–52 (2015)
27. Swain, K.C., Thomson, S.J., Jayasuriya, H.P.: Adoption of an unmanned helicopter for low-altitude remote sensing to estimate yield and total biomass of a rice crop. Trans. ASABE **53**(1), 21–27 (2010)
28. Zarco-Tejada, P.J., González-Dugo, V., Williams, L., Suárez, L., Berni, J.A., Goldhamer, D., Fereres, E.: A pri-based water stress index combining structural and chlorophyll effects: Assessment using diurnal narrow-band airborne imagery and the CWSI thermal index. Remote Sens. Environ. **138**, 38–50 (2013)
29. Zhao, T., Chen, Y., Ray, A., Doll, D.: Quantifying almond water stress using unmanned aerial vehicles (UAVs): Correlation of stem water potential and higher order moments of non-normalized canopy distribution. In: ASME 2017 International Design Engineering Technical Conferences and Computers and Information in Engineering Conference American Society of Mechanical Engineers (2017)
30. Zhao, T., Niu, H., de la Rosa, E., Doll, D., Wang, D., Chen, Y.: Tree canopy differentiation using instance-aware semantic segmentation, in 2018 ASABE Annual International Meeting American Society of Agricultural and Biological Engineers (2018)
31. Lelong, C., Burger, P., Jubelin, G., Roux, B., Labbé, S., Baret, F.: Assessment of unmanned aerial vehicles imagery for quantitative

monitoring of wheat crop in small plots. Sensors **8**(5), 3557–3585 (2008)
32. Xiang, H., Tian, L.: Method for automatic georeferencing aerial remote sensing (RS) images from an unmanned aerial vehicle (UAV) platform. Biosyst. Eng. **108**(2), 104–113 (2011)
33. Wang, D., Li, M.: Stochastic configuration networks: Fundamentals and algorithms. IEEE Trans. Cybern. **47**(10), 3466–3479 (2017)
34. Scardapane, S., Wang, D.: Randomness in neural networks: An overview. Wiley Interdisciplinary Reviews: Data Mining and Knowledge Discovery **7**, 2 (2017)
35. Niu, H., Wei, J., Chen, Y.: Optimal randomness for stochastic configuration network (scn) with heavy-tailed distributions. Entropy **23**(1), 56 (2021)
36. Broomhead, D., Lowe, D.: Multivariable functional interpolation and adaptive networks complex systems (1988)
37. Pao, Y.-H., Takefuji, Y.: Functional-link net computing: Theory, system architecture, and functionalities. Computer **25**(5), 76–79 (1992)
38. Wang, D., Li, M.: Deep stochastic configuration networks with universal approximation property. In: 2018 International Joint Conference on Neural Networks (IJCNN), pp. 1–8. IEEE (2018)
39. Li, M., Wang, D.: 2-D stochastic configuration networks for image data analytics. IEEE Transactions on Cybernetics (2019)
40. Wang, W., Wang, D.: Prediction of component concentrations in sodium aluminate liquor using stochastic configuration networks. Neural Comput. Applic., 1–14 (2020)
41. Lu, J., Ding, J., Dai, X., Chai, T.: Ensemble stochastic configuration networks for estimating prediction intervals: A simultaneous robust training algorithm and its application. IEEE Transactions on Neural Networks and Learning Systems (2020)
42. Huang, C., Huang, Q., Wang, D.: Stochastic configuration networks based adaptive storage replica management for power big data processing. IEEE Trans. Industr. Inform. **16**(1), 373–383 (2019)
43. Zhao, T., Yang, Y., Niu, H., Wang, D., Chen, Y.: Comparing U-Net convolutional network with mask R-CNN in the performances of pomegranate tree canopy segmentation. In: Multispectral, Hyperspectral, and Ultraspectral Remote Sensing Technology, Techniques and Applications VII International Society for Optics and Photonics (2018)

Publisher's Note Springer Nature remains neutral with regard to jurisdictional claims in published maps and institutional affiliations.

Haoyu Niu is a Ph.D. candidate in Electrical Engineering and Computer Science at the University of California, Merced. He is interested in Precision Agriculture, Big Data, Deep Learning, sUAS Remote Sensing/Application. He interned at the Lawrence Livermore National Lab (LLNL) in 2020 and 2021. He was also one of the Bayer's Grants4Ag Award recipients in 2021.

Tiebiao Zhao earned his Ph.D. degree in Mechanical Engineering from University of California, Merced, 2018, and MSc degree in Control Theory and Control Engineering from University of Science and Technology of China in 2012. His research interests include applications of small unmanned aerial systems (sUAS) in precision agriculture, especially water stress detection and yield prediction. His current research focuses on developing next-generation vegetation indices specifically for UAV-based remote sensing, characterized by high spatial resolution and high temporal resolution.

Dr. Dong Wang received his Ph.D. in Soil and Environmental Physics from University of Wisconsin Madison, M.Sc. in Agricultural Engineering from University of Idaho, and B.Eng. in Hydraulic Engineering from Beijing Agricultural Engineering University. Since 2006, Dr. Wang has been Supervisory Research Soil Scientist and Research Leader of the USDA ARS Water Management Research Unit, Parlier, CA. He and his research team are internationally recognized for research on developing effective and sustainable strategies for crop water management and alternatives to methyl bromide soil fumigation. Prior to joining ARS, Dr. Wang was professor in Department of Soil, Water, and Climate at the University of Minnesota, St. Paul, MN. Dr. Wang has conducted scientific research for over 30 years and received more than 100 invitations to speak at and chair national and international conferences, write books and book chapters, and serve on journal editorial boards and national and international scientific panels and technical committees. He has published more than 300 peer-reviewed journal articles, invited book chapters, and technical reports. Dr. Wang is a Fellow of the American Society of Agronomy and Soil Science Society of America.

YangQuan Chen is a full professor at the School of Engineering, University of California, Merced. He was on the faculty of Electrical and Computer Engineering Dept. of Utah State University, Logan, Utah from 2000 to 2012 where he was a tenured associate professor and the Director for the Center for Self-Organizing and Intelligent Systems (CSOIS) from 2004–2012. Dr. Chen published many books, papers and patents. He served as the General Co-Chair for ICUAS 2014 and 2017, 2019 (International Conference on Unmanned Aircraft Systems), and on the editorial board for journals like IEEE Trans. on Control Systems Technology, ISA Trans., ASME Journal of Dynamics Systems, Measurement and Control, IFAC journals of Control Engineering Practice as well as IFAC Mechatronics, Fractional Calculus and Applied Analysis, and Nonlinear Dynamics. He also serves as the Topical Editor-in-Chief (Field Robotics), International Journal of Advanced Robotics Systems (IJARS) and Intelligent Service Robotics. He serves as an editorial board member of MDPI Applied Sciences, Sensors. His ISI Publon H-index is 67 with more than 19.6k citations, GoogleScholar citation is 43.2k with H-index 91, H10-index 540. Dr. Chen was in the 2018, 2019, 2010 and 2021 Highly Cited Researchers List by Clarivate. He won Research of The Year awards from Utah State University (2012) and UC Merced (2020) respectively. In 2018, for his cumulative work in drones, Dr. Chen won "Senate Distinguished Scholarly Public Service award" that recognizes a faculty member who has energetically and creatively applied his or her professional expertise and scholarship to benefit the local, regional, national or international community.